Carbon 162 (2020) 382–391

Contents lists available at ScienceDirect

Carbon

journal homepage: www.elsevier.com/locate/carbon

Preparation and characterization of high damage-tolerance nacre-inspired magnesium alloy matrix composites with high carbon nanotube contents

Xun Sun [a, b], Rui-Fen Guo [b], Alateng Shaga [c], Zhi-Jie Hu [b], Ping Shen [a, b, *], Zhi-Qiang Zhang [b, **], Qi-Chuan Jiang [a, b]

[a] State Key Laboratory of Automotive Simulation and Control, Jilin University, PR China
[b] Key Laboratory of Automobile Materials (Ministry of Education), School of Materials Science and Engineering, Jilin University, No. 5988 Renmin Street, Changchun, 130025, PR China
[c] Department of Materials Science and Engineering, Jilin Jianzhu University, No. 5088 Xincheng Street, Changchun, 130118, PR China

ARTICLE INFO

Article history:
Received 28 November 2019
Received in revised form
16 February 2020
Accepted 23 February 2020
Available online 24 February 2020

ABSTRACT

A nacre-like magnesium matrix composite with high carbon nanotube (CNT) contents (up to 4.40 wt%) was successfully prepared under the combined effects of bidirectional freeze casting, pressureless infiltration, and hot pressing. The bidirectional freeze casting was carried out to fabricate large-scale parallelly layered CNT scaffolds. The spontaneous infiltration of an AZ91 magnesium alloy was achieved using nano-silica as the wetting promoter, and MgO and Mg_2Si (reaction products) provided the strength of the as-synthesized composites. Furthermore, the hot pressing increased the average thickness ratio of reinforcing phase/alloy layers in the AZ91/CNT composites from 0.89 (before hot pressing) to 1.46 (after hot pressing) and also significantly improved the specific strength from 142.3 MPa/(g·cm^{-3}) to 158.7 MPa/(g·cm^{-3}) without sacrificing the specific toughness ((17–18) MPa·m$^{1/2}$/(g·cm^{-3})). The resultant composites were mainly strengthened by CNTs, reaction products, and the strong interfacial bonding between CNTs and the Mg matrix. The key toughening mechanisms for the as-prepared composites were crack deflection, branching, and CNT pull-out. This study provides a new idea for the economical and efficient preparation of lightweight and damage-tolerant composites with high CNT contents.

1. Introduction

Strength and toughness are mutually exclusive in many traditional metal matrix composites (MMCs), and the achievement of ideal mechanical properties is invariably a compromise [1]. Therefore, developing a new structural composite that combines lightweight, high strength, and toughness has been a major challenge [2]. In order to meet this challenge, a rational solution lies in material selection and structural design.

In material selection, Mg and CNTs are ideal choices for the metal matrix and the reinforcement, respectively, due to their low densities (Mg: 1.7 g/cm^3, CNTs: about 1/6 of steel), high specific strengths, and specific stiffnesses [3–5]. Therefore, CNTs are generally incorporated into the Mg matrix to prepare lightweight, high-strength composites. In structural design, a feasible strategy can be achieved from biological materials. Many biological materials in nature possess a perfect combination of strength and toughness due to their complex and fine structures. A notable example is nacre. Its laminated structure formed by the alternating arrangement of brittle aragonite sheets (95 vol%, 200–900 nm thick) and biopolymer layers (5 vol%, 10–50 nm thick) can generate significantly higher strength and fracture toughness. Aragonite sheets ("brick") provide the necessary strength, whereas limited displacements (of few micrometers) within the bio-polymeric "mortar" dissipate locally generated high stresses, thereby providing a certain degree of ductility to improve the toughness. The preparation of nacre-inspired composites has attracted

* Corresponding author. State Key Laboratory of Automotive Simulation and Control, Jilin University, PR China.
** Corresponding author. Key Laboratory of Automobile Materials (Ministry of Education), School of Materials Science and Engineering, Jilin University, PR China.
E-mail addresses: shenping@jlu.edu.cn (P. Shen), zhangzq@jlu.edu.cn (Z.-Q. Zhang).

https://doi.org/10.1016/j.carbon.2020.02.072
0008-6223/

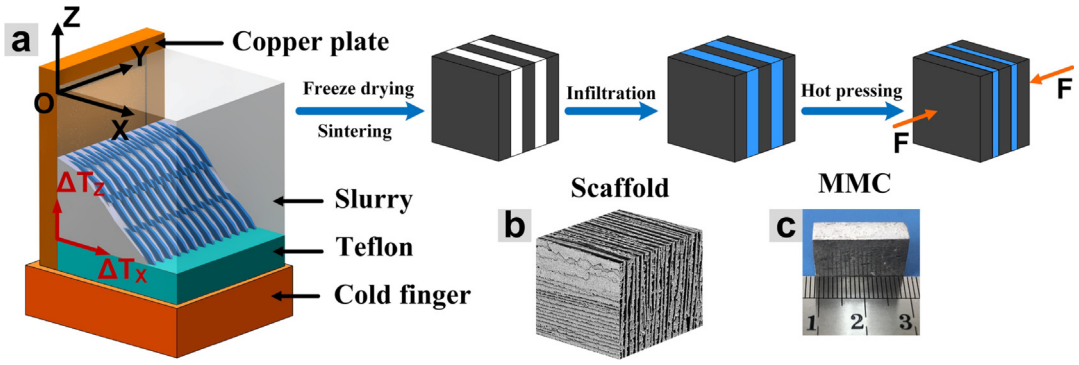

Fig. 1. (a) Schematic representation of the preparation route for AZ91/CNT composites, (b) 3D structure of the lamellar CNT scaffold, and (c) macroscopic morphology of the AZ91/CNT composites after hot pressing.

worldwide attention in the past decade [6–8]. For example, Xiang et al. [9] combined electrophoretic deposition (EPD) of CNTs with Mg foils to obtain Mg matrix composites with micro-nano layered structure, and prepared a nacre-like bulk Mg/CNT composite by hot-press sintering and hot rolling.

In 2006, Deville et al. [10] developed a nacre-inspired layered structure through freeze-casting. The directional growth of ice crystals was utilized to push ceramic particles to form a layered scaffold. Using freeze casting, Yan et al. [11] and Gutierrez et al. [12] successfully prepared layered CNT scaffolds, in which chitosan was used as dispersant and binder to provide the green strength of the scaffolds. The porosity of the resultant scaffolds reached 99% and 97%, respectively. Using the freeze-cast scaffold as a template, researchers have created numerous laminated composites with good mechanical properties through the infiltration technique [7,13–16].

The combination of ice templating and infiltration can effectively solve the problems of CNT damage, disordered arrangement, and uneven dispersion encountered in traditional processing (powder metallurgy or stir casting) of Mg/CNT composites [17–20]. However, it is difficult to synthesize laminated Mg/CNT composites through ice templating and infiltration due to the poor wettability of CNTs by molten Mg [21]. The most common method for improving the wettability is to coat CNT surfaces with metals (such as nickel); however, this process is complicated and the improvement in wettability is limited [22]. In order to solve this problem, in this study, SiO_2 was used as a wetting promoter due to the good wettability between Mg and SiO_2 [23,24]. SiO_2 favored the spontaneous infiltration of Mg into the layered silica-coated CNT scaffold and also provided the necessary strength for the CNT scaffold. Moreover, MgO and Mg_2Si (reaction products) improved the strength of the resultant composite. On the other hand, it was also found that the addition of Al to Mg can improve the interfacial bonding strength between CNTs and Mg [25]. Therefore, in the present experiment, an AZ91 (Mg–9Al–1Zn) alloy was selected as the metal matrix. Furthermore, the dispersion of CNTs in the water-based slurry was promoted by using chitosan as dispersant and binder (wet-dispersion), and CNTs were arranged and fixed in the metal through ice-templating and infiltration to solve the problem of uneven dispersion of CNTs and also to increase the CNT content for better mechanical properties of the resultant composite. However, the CNT content is usually kept low due to the restriction in slurry viscosity in freeze casting [11,12]. An effective way to increase the relative proportion of CNTs in the composites is to reduce the metal by hot-pressing the resultant composites. However, the hot pressing would crush randomly distributed ceramic layers formed by randomly nucleated ice crystals during freeze casting, thereby damaging the overall configuration and performance of the resultant composites. In order to solve this problem, a bidirectional freeze-casting technique [26] was adopted (i.e., the slurry directionally solidified under two temperature gradients to form a parallelly layered CNT scaffold).

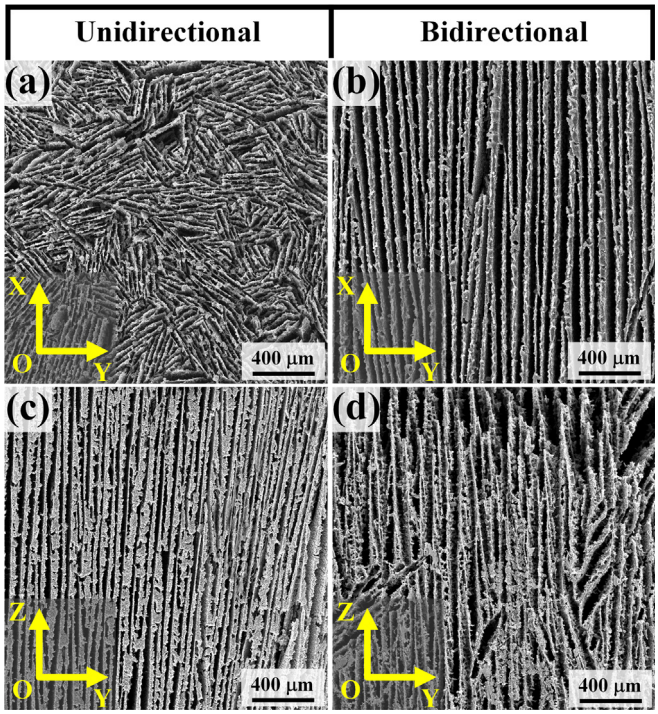

Fig. 2. SEM images of lamellar CNT scaffolds: (a) XOY and (c) ZOY sections of the unidirectionally freeze-cast sample; (b) XOY and (d) ZOY sections of the bidirectionally freeze-cast sample.

In the present work, laminated AZ91/CNT composites were prepared under the combined effects of bidirectional freezing, pressureless infiltration, and hot pressing. The effects of hot pressing on the interfacial structures and properties of the resultant composites were analyzed, and also their damage-resistant mechanisms were revealed. This study provides a new idea for the preparation of lightweight and damage-tolerant CNT-reinforced metal matrix composites.

2. Materials and methods

The main raw materials in the present experiment were commercial MWCNTs (diameter = 10–30 nm, length = 20–100 μm,

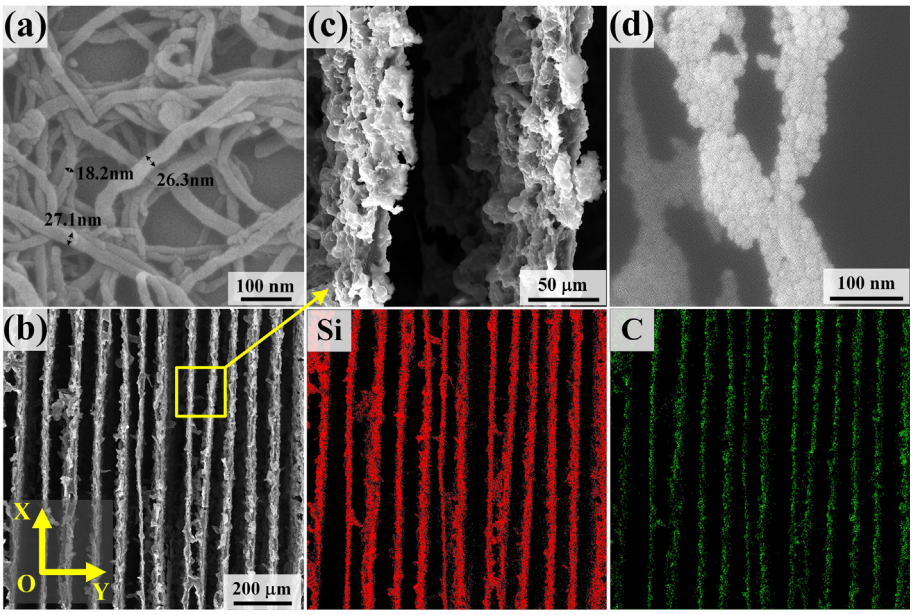

Fig. 3. (a) SEM image of as-received MWCNTs, (b) microstructure of the bidirectionally freeze-cast CNT scaffold in the XOY section, (c) magnified images of the area marked in image (b), and (d) enlarged view of image (c).

purity≥98%), silica sol (SiO_2 content = 30 wt%, particle size = 10–20 nm, pH = 2.0–4.0), and chitosan (CHI, purity 99.5%). MWCNTs (4 wt% of the slurry) and silica sol (SiO_2 accounted for 8 wt% of the slurry) were first dispersed in an acetic acid solution (0.2 mol/L) containing 1.5 wt% CHI. CHI is considered as an efficient dispersion agent for CNTs [12]. The acetic acid ensured that CHI was completely dissolved into a clear solution without an excess residue. A water-based CNT slurry was obtained by magnetic stirring (10 h) followed by ultrasonic dispersion (30 min) and vacuum deairing (30 min). The slurry was then poured into a bidirectional freeze-casting mold (Fig. 1a). A Teflon block was used to create thermal insulation between the slurry and the cold finger. When contacting the cold finger, the side copper plate generated two temperature gradients: a vertical one (ΔT_Z) and a horizontal one (ΔT_X). The ΔT_X gradient (along the X-axis) was the main growth direction for ice crystals, whereas the ΔT_Z gradient (along the Z-axis) was the secondary direction; hence, ice crystals grew into a parallelly layered structure [26]. The cold finger was then cooled down to 0 °C at 1 °C/min by a temperature controller until the slurry became completely frozen. The solidified slurry was demolded and freeze-dried at −50 °C (under a vacuum of 10 Pa) for 72 h to get a layered green body ($25 \times 25 \times 25$ mm^3). The body was first fired at 300 °C in air for 15 min to remove CHI and then sintered at 900 °C for 1 h under an Ar flow rate of 0.8 L/min. Fig. 1b displays the three-dimensional structure of the resultant scaffold.

A polished commercial AZ91 (Mg–9Al–1Zn) alloy was placed on the surface of the as-prepared scaffold. The samples were contained in a graphite crucible, whose internal surfaces were shielded by a graphite paper to prevent direct contact with the alloy. The furnace was evacuated to a vacuum of about 3 Pa, then purged with high-purity (99.999%) Ar, and finally, heated to 710 °C at 5 °C/min under an Ar flow rate of 0.8 L/min. The samples were held at 710 °C for 15 min to complete the spontaneous infiltration and then cooled to 20 °C at 5 °C/min. The as-prepared composites (with a CNT content of 2.29 wt%; the detailed calculation is presented in the Appendix) were cut into small pieces with a volume of $21 \times 21 \times 10$ mm^3, wrapped by graphite papers, and placed in a graphite mold for hot pressing. After heating to 650 °C for 15 min under an Ar (purity 99.999%) flow rate of 0.8 L/min, the samples were compressed to a maximum reduction of 5 mm and then cooled to 20 °C. The relative mass fraction of CNT in the AZ91/CNTs composites (Fig. 1c) reached 4.40 wt% (the detailed calculation is presented in the appendix).

The densities of the as-prepared composites and AZ91 alloy were measured by the Archimedes method. The elastic moduli and Poisson's ratios of the composites were determined by measuring the velocities of longitudinal and shear waves in the orthogonal direction with an ultrasonic thickness gauge (Olympus 38DL PLUS) [15]. The microstructural evolution in the composites was observed with an optical microscope (OM; Axio Imager A2m, Carl Zeiss, Germany), a scanning electron microscope (SEM; VEGA 3 XMU, TESCAN, Czech Republic), and a field-emission scanning electron microscope (JSM-6700F, Japan). The interfacial structures and phases of the composites were analyzed by transmission electron microscopy (TEM; JEM-2100F, Japan) and X-ray diffraction (XRD; D/Max 2500 PC Rigaku, Japan), respectively. The three-point flexural strength and fracture toughness of the composites were measured with a universal testing machine (Instron 5689, Instron Corp., USA). The properties of the AZ91 alloy after the infiltration experiment (taken from the remaining alloy on the top of the sample) were also measured under the same conditions to provide with contrastive reference. The flexural strength was measured using unnotched specimens (width = 4 mm, thickness = 3 mm, length = 20 mm) with a span of 16 mm at a loading rate of 0.5 mm/min. The fracture toughness was measured using single-edge notched bending (SENB) samples (width = 4 mm (W), thickness = 2 mm (B), length = 20 mm, notch depth = 2 mm (a)) with a span 16 mm at a crosshead speed of 0.05 mm/min. The values of crack-initiation toughness (K_{IC}), crack-growth toughness (K_{JC}), and work of fracture (U) were calculated using the following equations [27]:

$$K_{IC} = \frac{PS}{BW^{\frac{3}{2}}} f\left(\frac{a}{w}\right), \quad (1)$$

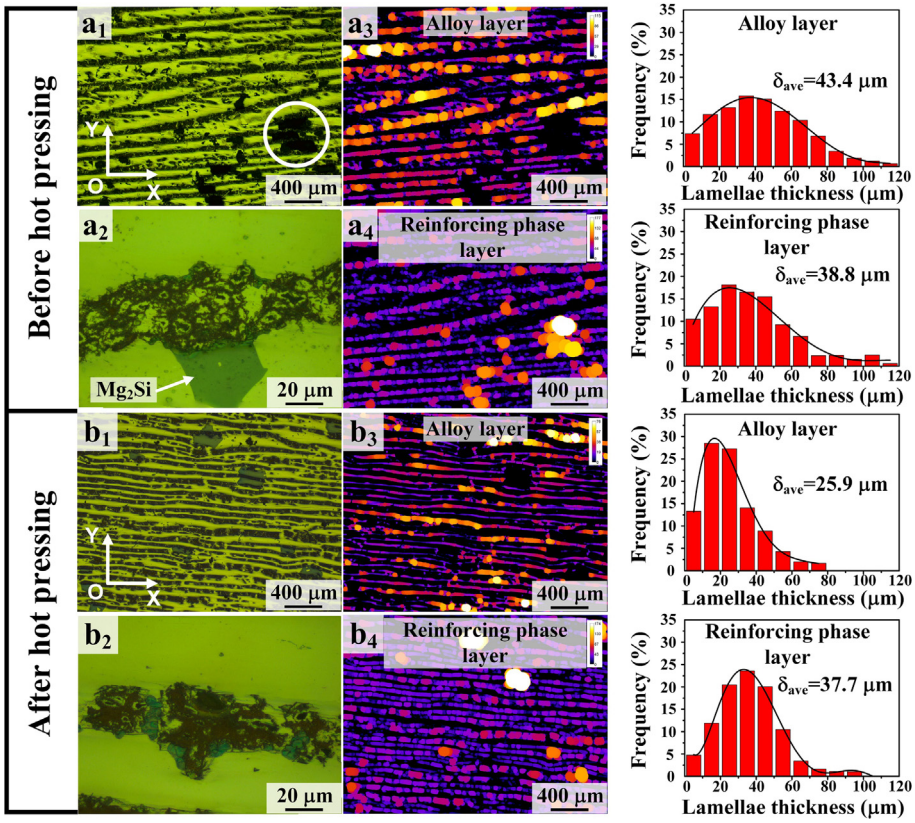

Fig. 4. Microstructures of the AZ91/CNT composites before (a_1–a_2) and after (b_1–b_2) hot pressing; lamellae thickness distributions and statistical plots obtained by image analysis for the composites before (a_3–a_4) and after (b_3–b_4) hot pressing. See color in electronic file.

$$K_{JC} = \sqrt{\left(J_{el} + J_{pl}\right)E'}, \tag{2}$$

$$f\left(\frac{a}{w}\right) = \frac{3\left(\frac{a}{w}\right)^{\frac{1}{2}}\left[1.99 - \frac{a}{w}\left(1 - \frac{a}{w}\right)\left(2.15 - 3.93\frac{a}{w} + 2.7\left(\frac{a}{w}\right)^2\right)\right]}{2\left(1 + 2\frac{a}{w}\right)\left(1 - \frac{a}{w}\right)^{\frac{3}{2}}}, \tag{3}$$

$$J_{el} = \frac{K_{IC}^2}{E'}, \tag{4}$$

$$J_{pl} = \frac{1.9A_{pl}}{Bb}, \tag{5}$$

$$E' = \frac{E}{1 - \nu^2}, \tag{6}$$

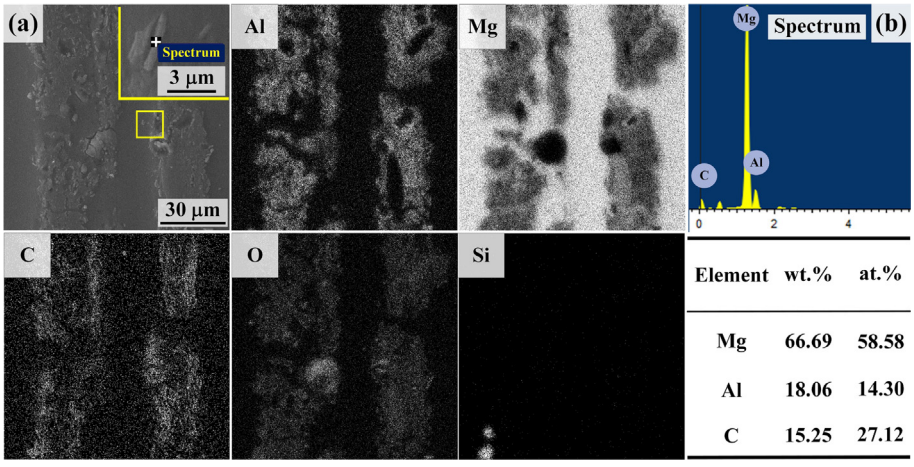

Fig. 5. (a) BSE image and elemental mappings of the AZ91/CNT composites after hot pressing and (b) point analysis result (the point-analysis spot is shown in the upper right frame of Fig. 5a).

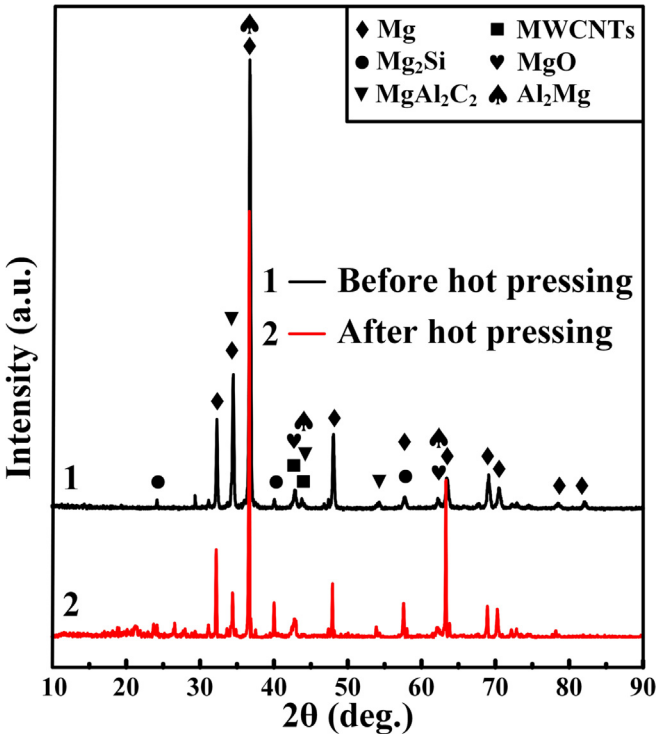

Fig. 6. XRD patterns for the AZ91/CNT composites before and after hot pressing.

$$U = \frac{A_{pl}}{2A}, \tag{7}$$

where P is the maximum applied load, A_{pl} is the area of the plastic zone under the load–displacement curve, and b is the uncracked ligament length (W–a). The final value presented here was the average of at least three measurements.

3. Results and discussion

3.1. Microstructures of lamellar CNT scaffolds

Fig. 2 displays the microstructures of lamellar CNT scaffolds prepared by unidirectional and bidirectional freeze casting. The slurry and the freezing rate (1 °C/min) were the same in both cases. During unidirectional freeze casting, the slurry was in direct contact with the cold finger. With the decrease in the cold finger temperature, a single vertical temperature gradient (ΔT_Z) was created; thus forcing ice crystals to grow into a layered structure from bottom to top (Fig. 2c). However, as the random nucleation of ice crystals occurred on the entire surface of the cold finger, the lamellar orientation over the XOY plane was random (Fig. 2a).

During bidirectional freeze casting, ice crystals grew along two directions (Fig. 1a). Hence, after freeze-drying and sintering, a large-scale parallelly layered structure was obtained (Fig. 2b and d). It indicates that bidirectional freezing controlled the arrangement of ice crystals in both directions, whereas unidirectional freezing was limited to only one direction. From the standpoint of preparing high-CNT-content composites, such large-scale parallelly layered structures would be certainly superior to those obtained by unidirectional freeze casting to maintain the structural integrity in subsequent hot pressing.

Raw CNT powders had a relatively uniform outer diameter and a large aspect ratio; however, they were easily entangled and difficult to be dispersed (Fig. 3a). The entanglement of CNTs significantly influenced the dispersion of CNTs in the melt [17]. Here, the CNT powders were pre-dispersed in the CHI slurry due to the non-covalent association of CNTs with CHI chains in the aqueous solution [12]. The bidirectional freezing of the slurry led to the directional arrangement of the CNT lamellae. The CNT layers maintained good parallelism with a uniform thickness in the XOY section (~20 mm away from the bottom) (Fig. 3b). The elemental

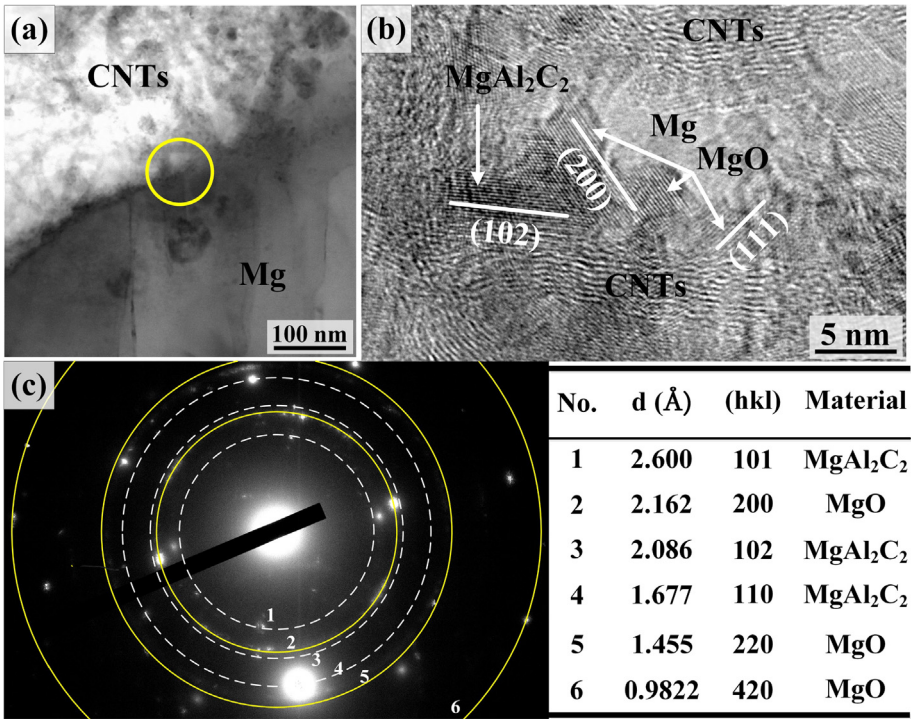

No.	d (Å)	(hkl)	Material
1	2.600	101	$MgAl_2C_2$
2	2.162	200	MgO
3	2.086	102	$MgAl_2C_2$
4	1.677	110	$MgAl_2C_2$
5	1.455	220	MgO
6	0.9822	420	MgO

Fig. 7. (a) TEM image of the AZ91/CNT composites after hot pressing, (b) HRTEM image of the interface between the Mg matrix and CNTs, and (c) SAED pattern of the corresponding area marked in image (a) and the phase corresponding to each diffraction ring.

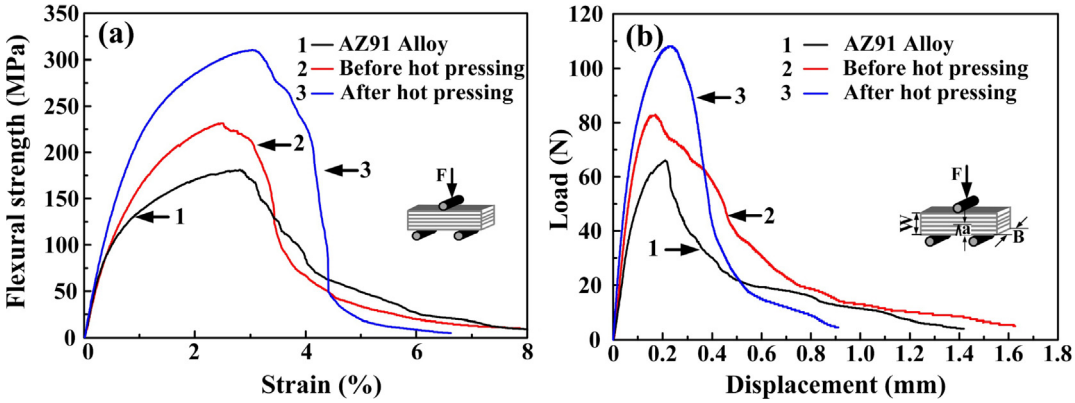

Fig. 8. Three-point bending (a) stress–strain and (b) load–displacement curves of the AZ91 alloy and the AZ91/CNT composites before and after hot pressing.

mapping of the CNT scaffold reveals that SiO_2 were evenly distributed in the CNT lamellae. The enlarged view in Fig. 3d indicates that CNTs were coated with the nano-sized SiO_2 particles (10–20 nm; denoted as SiO_2@CNTs), which contributed to the spontaneous infiltration as SiO_2 was well wetted by Mg [23,24]. In addition, SiO_2@CNTs layers contained many tiny pores (Fig. 3c). The filling of these pores by the melt increased the contact area between SiO_2 and Mg and promoted the interfacial reaction.

3.2. Microstructures of AZ91/CNT composites

Fig. 4a_1 and a_2 presents the microstructures of AZ91/CNT composite along the XOY section before hot pressing (the reinforcing phase layers and alloy layers appeared as black and green, respectively, and the blue-green block was Mg_2Si [28]). CNTs were regularly distributed in the metal matrix, thus avoiding the problem of local accumulation encountered in conventional methods (such as stir casting) [20]. Reinforcing phase layers were continuous, and some defects, such as pores and incompletely filled areas, appeared between these layers (marked by circles in Fig. 4a_1). Bulk Mg_2Si was adhered to the reinforcing phase layers; the alloy penetrated into the tiny pores of these layers, and reaction products were wrapped around filamentous CNTs to form a network structure (Fig. 4a_2). This phenomenon suppressed the deformation of the reinforcing phase layers by hindering the sliding of reaction products and increased elastic modulus [29]. Fig. 4a_3 and 4a_4 displays the layer thickness distribution and statistical plots calculated by Fiji software. The average thicknesses of the reinforcing phase layers and the alloy layers were calculated as 38.8 μm and 43.4 μm, respectively (the ratio was 0.89).

Fig. 4b_1 and b_2 show the microstructures of the AZ91/CNT composites along the XOY section after hot pressing. It was found that no obvious defects were formed due to hot pressing. Fig. 4b_1 reveals that the reinforcing phase layers became discontinuous after hot pressing. Moreover, the morphology of the resultant composites changed from lamellar to "brick-mortar" after hot pressing. The structure shown in Fig. 4b_2 was denser than that in Fig. 4a_2 due to the reduction in the alloy content in the reinforcing phase layers. Fig. 4b_3 and b_4 show that the average thickness of alloy layers was reduced to 25.9 μm, whereas the thickness ratio of the reinforcing-phase/alloy layers increased to 1.46. This result indicates that the hot pressing significantly increased the relative mass fraction of the reinforcing phases. In addition, the layer thickness distribution curves imply that the thicknesses of the reinforcing phase layers and the alloy layers became more uniform after hot pressing.

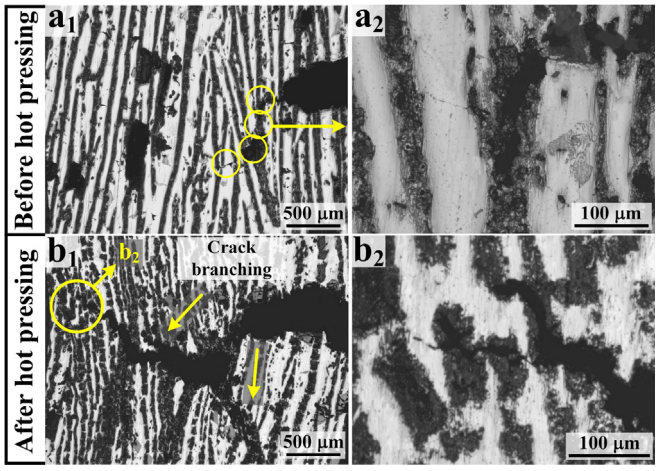

Fig. 9. Optical microscopy images showing crack propagation in the AZ91/CNT composites before (a_1–a_2) and after (b_1–b_2) hot pressing during bending tests (The circle in image a_1 marks the direction of crack propagation; image a_2 is the enlarged view of the area marked in image a_1, and image b_2 is the enlarged view of the area marked in image b_1).

3.3. Phases of AZ91/CNT composites

Fig. 5 displays the SEM images and EDS spectra of the AZ91/CNT composites. When the molten Mg penetrated into the CNT scaffold,

Table 1
Physical [density (ρ), Poisson's ratio (ν), elastic modulus (E)] and mechanical [flexural strength (FS), crack-initiation toughness (K_{IC}), crack-growth toughness (K_{JC}), work of fracture (U)] properties of the matrix alloy and the AZ91/CNT composites before and after hot pressing (HP).

Specimens	ρ (g/cm^3)	ν	E (GPa)	FS (MPa)	K_{IC} (MPa·m$^{1/2}$)	K_{JC} (MPa·m$^{1/2}$)	U (kJ·m^{-2})
AZ91 alloy[a]	1.81 ± 0.01	0.295	45.8	170 ± 21	5.5 ± 0.2	32.5 ± 3.7	5.4 ± 1.2
Before HP	1.82 ± 0.01	0.272	48.7	259 ± 31	7.0 ± 0.9	32.6 ± 3.2	5.1 ± 1.4
After HP	1.89 ± 0.03	0.243	56.7	300 ± 10	7.8 ± 1.4	33.7 ± 3.6	4.7 ± 1.0

[a] The alloy for the measurement was taken from the top additional part after infiltration.

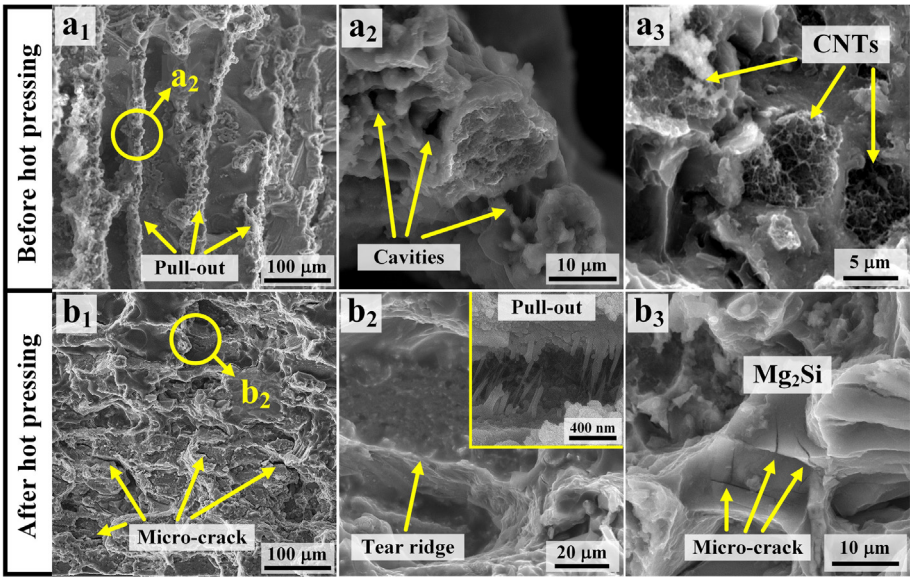

Fig. 10. Typical bending fracture surface morphologies of the AZ91/CNT composites before (a_1–a_3) and after (b_1–b_3) hot pressing (a_2 and a_3 are the enlarged views of a_1; b_2 and b_3 are the enlarged views of b_1).

it first reacted with SiO_2 on the CNT surface.

$$4Mg + SiO_2 \rightarrow 2MgO + Mg_2Si. \quad (8)$$

The distributions of Mg and O reveal that a large amount of MgO was formed and uniformly distributed in the reinforcing phase layers. The distribution of Si indicates that Mg_2Si accumulated in the local area. In addition, Al in the AZ91 alloy diffused to the reinforcing phase layers, indicating that Al was actively involved in the reaction. The elemental point analysis (Fig. 5b) of the local region in Fig. 5a reveals that the acicular phase was composed of binary or ternary compounds of Mg, Al, and C.

The XRD patterns for the resultant composites are illustrated in Fig. 6. Mg_2Si, MgO, and $MgAl_2C_2$ were the main reaction products. The formation of these phases increased the strength and simultaneously, damaged the toughness of the as-prepared composites. The diffraction peak of SiO_2 was not detected, indicating that the reaction was complete under the condition of excessive Mg. In addition, the intensities of the Mg peaks decreased while those of Mg_2Si increased significantly after hot pressing, suggesting that the Mg content decreased and the relative mass fraction of reaction products increased after the hot pressing.

In order to examine the formation of reaction products in the AZ91/CNT composites, the interfacial structures were revealed by TEM (Fig. 7). The interface between the reinforcing phase and the alloy was clear (Fig. 7a). The diffraction rings of the SAED pattern shown in Fig. 7c indicate that $MgAl_2C_2$ was formed at the interface; thus Al diffused from the AZ91 matrix to CNTs and agglomerated at the surface. However, considering the stable structure of CNTs, the carbon source for the reaction might also come from the amorphous carbon formed from the thermal decomposition of CHI during the sintering of the green body. Fukuda et al. [30] also confirmed the existence of $MgAl_2C_2$ in AZ61 (Mg–6Al–1Zn)/CNT composites fabricated by powder metallurgy through TEM examination. In addition, the HRTEM image around CNTs in Fig. 7b displays the presence of a large number of nanoscale MgO. MgO had good interfacial bonding with CNTs and Mg and improved the strength of the resultant composites [31]. The formation of $MgAl_2C_2$ and MgO increased the interfacial bonding strength between CNTs and Mg. The interfacial shear stress in Mg was effectively transferred to CNTs and reaction products under loading, thereby reducing the stress in the matrix and strengthening the composites by load transfer [32].

3.4. Mechanical properties of AZ91/CNT composites

Fig. 8 shows the three-point bending stress–strain and load–displacement curves of AZ91 alloy and the AZ91/CNT composites before and after hot pressing. The values of flexural strength (FS), crack-initiation toughness (K_{IC}), crack-growth toughness (K_{JC}), fracture work (U), and some physical properties are given in Table 1. In comparison to the alloy, the FS of the composites before and after hot pressing increased by 52.4% and 76.5%, respectively, whereas the fracture strain remained the same. Furthermore, the FS of the composites displayed a gradually decreasing behavior rather than a sudden catastrophic drop, indicating the occurrence of macroscopic plastic deformation and stable crack propagation. In most engineering materials, strength and toughness are mutually exclusive; hence, the achievement of the optimal performance invariably imposes compromise. However, the simultaneous increase in strength and toughness was noticed in the AZ91/CNT composites after hot pressing. The significant increase in the flexural strength can be attributed to the increase in the relative proportion of CNTs and other reinforcing phases (Mg_2Si, MgO, $MgAl_2C_2$, and Al_2Mg) in the composites. Goh et al. [33] reported that the hot pressing might deteriorate the toughness of composites with increasing ceramic content. The elongation of the composites prepared by traditional methods sharply decreases with increasing CNT content [5]. In the present work, the increased toughness of the AZ91/CNT composites after hot pressing could be ascribed to the improvement in the relative mass fraction of CNTs, the orderly arrangement of CNTs, and the reduction in defects.

Density is another important property for structural materials. Therefore, specific strength and specific toughness are two key factors to evaluate the performance of a material. The densities of the AZ91/CNT composites before and after hot pressing reached 1.82–1.89 g/cm^3 (close to that of the AZ91 alloy). The specific strength and specific toughness of the AZ91/CNT composites after hot pressing were calculated as 158.7 MPa/(g·cm^{-3}) and 17.8 MPa·m$^{1/2}$/(g·cm^{-3}), respectively. The specific toughness of the

AZ91/CNT composites after hot pressing was about 4.6 and 2.4 times that of Al_2O_3 fiber-reinforced magnesium matrix composites (3.9 MPa·$m^{1/2}$/(g·cm^{-3}) [34]) and AZ91/$Mg_2B_2O_5$w laminated composites (7.3 MPa·$m^{1/2}$/(g·cm^{-3}) [28]), respectively. Moreover, the AZ91/CNT composites yielded higher specific modulus (E/ρ~30 GPa/(g·cm^{-3})), specific strength (158.7 MPa/(g·cm^{-3})), and specific toughness (17.8 MPa·$m^{1/2}$/(g·cm^{-3})) than titanium alloy (E/ρ~26 GPa/(g·cm^{-3}), 139.5 MPa/(g·cm^{-3}), and 13.4 MPa·$m^{1/2}$/(g·cm^{-3}), respectively [35]).

3.5. Fracture behavior of AZ91/CNT composites

Fig. 9 shows the crack propagation in the AZ91/CNTs composites during bending tests before and after hot pressing. It is observable that the main crack propagation direction was perpendicular to the arrangement direction of the metal and reinforcing phase layers. The composites before hot pressing had obvious crack deflection (Fig. 9a_1), and the crack propagated along the reinforcing phase layer (Fig. 9a_2). The crack deflection angle was close to 90° (extending along the reinforcing layer). The crack deflection angle in the composites after hot pressing remained the same; however, the number of crack deflections (Fig. 9b_1) and the branching on the main crack (marked by arrows in Fig. 9b_1) increased significantly. At the crack tip, the crack deflected along the reinforcing phase layer and the brittle "brick" deviated from its original position (Fig. 9b_2). In the "brick-mortar" structure, the complex plastic deformation of the ductile phase occurred around the brittle "brick" when the crack propagated from the brittle layer to the ductile layer, thus dissipating local high stresses and hindering the further extension of the crack. Hence, the toughness of the composites after hot pressing did not decrease with the increase in the relative mass fraction of the reinforcing phases. Therefore, the exceptional toughness of the AZ91/CNT composites can be attributed to crack deflection, branching, blunting, and brittle "brick" displacement. In addition, the crack deflection in the reinforcing phase layers indicates the presence of a strong interface between CNTs and Mg due to the formation of reaction products ($MgAl_2C_2$ and MgO); thus the interfacial shear stress was effectively transferred from Mg to CNTs under loading, leading to a higher strength [32]. Therefore, the strong interfacial bonding and the increased relative mass fraction of reinforcing phases (CNTs and reaction products) were the main sources for the strengthening of the AZ91/CNT composites.

Fig. 10 displays typical bending fracture surfaces of the AZ91/CNT composites before and after hot pressing. Due to the better plasticity of the thicker alloy layer before hot pressing, the considerable toughness of the AZ91/CNT composites was associated with crack front convolution [36]. In addition, the pull-out of the reinforcing phase layers (Fig. 10a_1, a_2) might be related to the presence of defects in local areas within or between the layers (Fig. 10a_2), thus resulting in the weak interface between the alloy layers and the reinforcing phase layers. Consequently, the interface became debonded during fracture. In contrast, defects in the composites were eliminated after hot pressing; therefore, the pull-out of reinforcing phase layers did not occur (Fig. 10b_1). The excellent toughness of the AZ91/CNT composites after hot pressing can be attributed to crack branching (the formation of microcracks in Fig. 10b_1), the deformation of the alloy (the formation of tearing ridges in Fig. 10b_2), and the pull-out of CNTs (the enlarged view of Fig. 10b_2). When CNTs were pulled out (similar to aragonite sheets in nacre [6]), the interfacial debonding between CNTs and the matrix consumed a lot of fracture energy, slowed the crack propagation, and played an important role in toughening [32]. Xiang et al. [9] also observed the similar phenomenon and explained the improvement of the composite properties with the "CNTs pull-out" mechanism. In addition, some microcracks were observed in the brittle phase (Mg_2Si) (Fig. 10b_3); hence, large-sized Mg_2Si acted as a source of crack propagation and reduced the toughness [24]. Therefore, it is necessary to control the degree of interfacial reactions and prevent the excessive growth of Mg_2Si.

4. Conclusions

In the present study, laminated magnesium matrix composites with high CNT contents were prepared under the combined effects of bidirectional freeze casting, pressureless infiltration, and hot pressing. The main observations are presented below:

1. Using SiO_2 as a wetting promoter, the spontaneous infiltration of Mg in the layered CNT scaffold was achieved. MgO and Mg_2Si (reaction products) enhanced the strength of the resultant composites.
2. The ordered alignment of CNTs in the resultant composites provided excellent damage tolerance with a specific strength of 158.7 MPa/(g·cm^{-3}) and a specific toughness of 17.8 MPa·$m^{1/2}$/(g·cm^{-3}) after hot pressing.
3. The resultant composites were mainly strengthened by CNTs, reaction products, and the strong interfacial bonding between CNTs and the Mg matrix. The composites were externally toughened by crack deflection, branching, and CNT pull-out.

Declaration of competing interest

The authors declare that they have no known competing financial interests or personal relationships that could have appeared to influence the work reported in this paper.

CRediT authorship contribution statement

Xun Sun: Methodology, Software, Visualization, Data curation, Investigation, Writing - original draft. **Rui-Fen Guo:** Methodology, Visualization, Writing - review & editing. **Alateng Shaga:** Funding acquisition. **Zhi-Jie Hu:** Methodology, Software, Visualization. **Ping Shen:** Conceptualization, Methodology, Visualization, Resources, Supervision, Funding acquisition. **Zhi-Qiang Zhang:** Supervision. **Qi-Chuan Jiang:** Supervision.

Acknowledgments

This work is supported by the National Key R&D Plan (No. 2017YFB0703101), the National Natural Science Foundation of China (No. 51901084, 51571099 and 51801070), the Changbai Mountain Scholars Program of Jilin Province (No. 2015011), and the 13th 5-year Science & Technology Research Program of the Department of Education of Jilin Province (No. JJKH20180579KJ).

Appendix

1. Calculation of CNT mass fraction in the AZ91/CNT composite before hot pressing:

The following assumptions were made during the calculation: (1) the volume of the green body during sintering did not shrink, (2) the AZ91 alloy filled all pores during pressureless infiltration, (3) only the reaction between SiO_2 and Mg occurred, and (4) SiO_2 disappeared after the reaction. The mass fractions of CNTs (ω_{CNTs}), MgO (ω_{MgO}), Mg_2Si (ω_{Mg2Si}), and AZ91 (ω_{AZ91}) were calculated using the following equations:

$$m_{MMC} = m_{CNTs} + m_{MgO} + m_{Mg_2Si} + m_{AZ91}, \quad (1)$$

$$m_{AZ91} = \rho_{AZ91}\left(V_{Porosity} - V_{Mg} - \Delta V_{Reaction}\right), \quad (2)$$

$$V_{Porosity} = V_{H_2O} + m_{CHI}/\rho_{CHI}, \quad (3)$$

$$\Delta V_{Reaction} = m_{MgO}\Big/\rho_{MgO} + m_{Mg_2Si}\Big/\rho_{Mg_2Si} - m_{SiO_2}\Big/\rho_{SiO_2} - V_{Mg}, \quad (4)$$

where m_{CNTs} and m_{SiO2} are the addition amounts of CNTs and SiO_2 in the slurry, respectively, and V_{Mg} is the volume of Mg involved in the following reaction:

$$4Mg + SiO_2 \rightarrow 2MgO + Mg_2Si. \quad (5)$$

The mass fractions of CNTs, MgO, Mg_2Si, and AZ91 were calculated as 2.29 wt%, 6.14 wt%, 5.85 wt%, and 85.72 wt%, respectively. The volume fraction of the reinforcing phases (φ) was calculated as 13.81 vol% using Equation (6):

$$\varphi = 1 - \omega_{AZ91}\rho_{MMC}/\rho_{AZ91}, \quad (6)$$

where ρ_{AZ91} (1.81 g/cm^3) and ρ_{MMC} (1.82 g/cm^3) are the densities of AZ91 alloy and AZ91/CNTs composites before hot pressing, respectively.

2. Calculation of CNT mass fraction in the AZ91/CNT composite after hot pressing

It was assumed that only AZ91 alloy was extruded during hot pressing, and the mass of the reinforcing phases (CNTs and reaction products) remained unchanged. The masses of as-prepared composites before and after hot pressing were denoted as M_1 and M_2, respectively. The mass fractions of CNTs (ω'_{CNTs}), MgO (ω'_{MgO}), Mg_2Si (ω'_{Mg2Si}), and AZ91 (ω'_{AZ91}) were calculated by the following equations:

$$\omega'_{CNTs} = \omega_{CNTs}M_1/M_2 \quad (7)$$

$$\omega'_{MgO} = \omega_{MgO}M_1/M_2 \quad (8)$$

$$\omega'_{Mg_2Si} = \omega_{Mg_2Si}M_1\Big/M_2 \quad (9)$$

$$\omega'_{AZ91} = 1 - \omega'_{CNTs} - \omega'_{MgO} - \omega'_{Mg_2Si}. \quad (10)$$

The mass fractions of CNTs, MgO, Mg_2Si, and AZ91 were calculated as 4.40 wt%, 11.79 wt%, 11.24 wt%, and 72.57 wt%, respectively. The volume fraction of the reinforcing phases (φ') was calculated as 24.22 vol% by Equation (11):

$$\varphi' = 1 - \omega'_{AZ91}\rho'_{MMC}/\rho_{AZ91}, \quad (11)$$

where ρ_{AZ91} (1.81 g/cm^3) and ρ'_{MMC} (1.89 g/cm^3) are the densities of the AZ91 alloy and the AZ91/CNTs composites after hot pressing, respectively.

References

[1] R.O. Ritchie, The conflicts between strength and toughness, Nat. Mater. 10 (2011) 817–822.
[2] J. Cho, A.R. Boccaccini, M.S.P. Shaffer, Ceramic matrix composites containing carbon nanotubes, J. Mater. Sci. 44 (2009) 1934–1951.
[3] T.M. Pollock, Weight loss with magnesium alloys, Science 328 (2010) 986–987.
[4] S.I. Yengejeh, M.A. Zadeh, A. Oechsner, On the tensile behavior of heterojunction carbon nanotubes, Composites, Part B 75 (2015) 274–280.
[5] Y. Shimizu, S. Miki, T. Soga, I. Itoh, H. Todoroki, T. Hosono, et al., Multi-walled carbon nanotube-reinforced magnesium alloy composites, Scripta Mater. 58 (2008) 267–270.
[6] U.G.K. Wegst, H. Bai, E. Saiz, A.P. Tomsia, R.O. Ritchie, Bioinspired structural materials, Nat. Mater. 14 (2015) 23–36.
[7] A.R. Studart, Towards high-performance bioinspired composites, Adv. Mater. 24 (2012) 5024–5044.
[8] M.A. Meyers, P.Y. Chen, M.I. Lopez, Y. Seki, A.Y. Lin, Biological materials: a materials science approach, J. Mech. Behav. Biomed. Mater. 4 (2011) 626–657.
[9] Y.Y. Xiang, X.J. Wang, X.S. Hu, L.L. Meng, Z.X. Song, X.J. Li, et al., Achieving ultra-high strengthening and toughening efficiency in carbon nanotubes/magnesium composites via constructing micro-nano layered structure, Composites, Part A 119 (2019) 225–234.
[10] S. Deville, E. Saiz, R.K. Nalla, A.P. Tomsia, Freezing as a path to build complex composites, Science 311 (2006) 515–518.
[11] J. Yan, H.R. Wang, T.H. Wu, X.K. Li, Z.Z. Ding, Elastic and electrically conductive carbon nanotubes/chitosan composites with lamellar structure, Composites, Part A 67 (2014) 1–7.
[12] M.C. Gutierrez, M.J. Hortigüela, J.M. Amarilla, R. Jiménez, M.L. Ferrer, F. Del Monte, Macroporous 3D architectures of self-assembled MWCNT surface decorated with Pt nanoparticles as anodes for a direct methanol fuel cell, J. Phys. Chem. C 111 (2007) 5557–5560.
[13] M.E. Launey, E. Munch, D.H. Alsem, H.B. Barth, E. Saiz, A.P. Tomsia, et al., Designing highly toughened hybrid composites through nature-inspired hierarchical complexity, Acta Mater. 57 (2009) 2919–2932.
[14] V. Naglieri, B. Gludovatz, A.P. Tomsia, R.O. Ritchie, Developing strength and toughness in bio-inspired silicon carbide hybrid materials containing a compliant phase, Acta Mater. 98 (2015) 141–151.
[15] A. Shaga, P. Shen, C. Sun, Q.C. Jiang, Lamellar-interpenetrated Al–Si–Mg/SiC composites fabricated by freeze casting and pressureless infiltration, Mater. Sci. Eng., A 630 (2015) 78–84.
[16] M.Q. Sun, P. Shen, Q.C. Jiang, Microstructures and mechanical characterizations of high-performance nacre-inspired Al/Al_2O_3 composites, Composites, Part A 121 (2019) 465–473.
[17] J.P. Salvetat, S. Bhattacharyya, R.B. Pipes, Progress on mechanics of carbon nanotubes and derived materials, J. Nanosci. Nanotechnol. 6 (2006) 1857–1882.
[18] H. Mindivan, A. Efe, A.H. Kosatepe, E.S. Kayali, Fabrication and characterization of carbon nanotube reinforced magnesium matrix composites, Appl. Surf. Sci. 318 (2014) 234–243.
[19] S.L. Xiang, X.J. Wang, M. Gupta, K. Wu, X.S. Hu, M.Y. Zheng, Graphene nanoplatelets induced heterogeneous bimodal structural magnesium matrix composites with enhanced mechanical properties, Sci. Rep. 6 (2016) 38824–38836.
[20] C.D. Li, X.J. Wang, K. Wu, W.Q. Liu, S.L. Xiang, C. Ding, et al., Distribution and integrity of carbon nanotubes in carbon nanotube/magnesium composites, J. Alloys Compd. 612 (2014) 330–336.
[21] E. Carreño-Morelli, J. Yang, E. Couteau, K. Hernadi, J.W. Seo, C. Bonjour, et al., Carbon nanotube/magnesium composites, Phys. Status Solidi 201 (2004) 53–55.
[22] S.N. Li, S.Z. Song, T.Q. Yu, Properties and microstructure of carbon nanotubes/magnesium matrix composites, J. Wuhan Univ. Technol. 25 (2003) 1–4.
[23] L.X. Shi, P. Shen, D. Zhang, E.T. Dong, Q.C. Jiang, Reactive wetting in liquid magnesium/silica and magnesium/silicon systems, Appl. Surf. Sci. 274 (2013) 124–130.
[24] H. Zhang, P. Shen, A. Shaga, R.F. Guo, Q.C. Jiang, Preparation of nacre-like composites by reactive infiltration of a magnesium alloy into porous silicon carbide derived from ice template, Mater. Lett. 183 (2016) 299–302.
[25] H. Fukuda, K. Kondoh, J. Umeda, B. Fugetsu, Fabrication of magnesium based composites reinforced with carbon nanotubes having superior mechanical properties, Mater. Chem. Phys. 127 (2011) 451–458.
[26] Z.J. Hu, X.T. Shen, S.L. Geng, P. Shen, Q.C. Jiang, 3D long-range ordered porous ceramics prepared by a novel bidirectional freeze-casting technique, Ceram. Int. 44 (2018) 5803–5806.
[27] M.E. Launey, E. Munch, D.H. Alsem, E. Saiz, A.P. Tomsia, R.O. Ritchie, A novel biomimetic approach to the design of high-performance ceramic–metal composites, J. R. Soc. Interface 7 (2009) 741–753.
[28] H.R. Mao, P. Shen, Y.H. Liu, Y.G. Zhao, Q.C. Jiang, Nacre-inspired lightweight and high-strength AZ91D/$Mg_2B_2O_5$w composites prepared by ice templating and pressureless infiltration, J. Mater. Sci. 53 (2018) 12167–12177.
[29] P. Lv, X.W. Tan, K.H. Yu, R.L. Zheng, J.J. Zheng, W. Wei, Super-elastic graphene/carbon nanotube aerogel: a novel thermal interface material with highly thermal transport properties, Carbon 99 (2016) 222–228.
[30] H. Fukuda, K. Kondoh, J. Umeda, B. Fugetsu, Interfacial analysis between Mg matrix and carbon nanotubes in Mg–6 wt.% Al alloy matrix composites reinforced with carbon nanotubes, Compos. Sci. Technol. 71 (2011) 705–709.
[31] Q.H. Yuan, X.S. Zeng, Y. Liu, L. Luo, J.B. Wu, Y.C. Wang, et al., Microstructure and mechanical properties of AZ91 alloy reinforced by carbon nanotubes coated with MgO, Carbon 96 (2016) 843–855.
[32] Q. Li, A. Viereckl, C.A. Rottmair, R.F. Singer, Improved processing of carbon nanotube/magnesium alloy composites, Compos. Sci. Technol. 69 (2009) 1193–1199.
[33] C.S. Goh, M. Gupta, J. Wei, L.C. Lee, Characterization of high performance Mg/

MgO nanocomposites, J. Compos. Mater. 41 (2007) 2325–2335.
[34] S. Jayalakshmi, S.V. Kailas, S. Seshan, K.B. Kim, E. Fleury, Tensile strength and fracture toughness of two magnesium metal matrix composites, J. Ceram. Process. Res. 7 (2006) 261–265.
[35] M.F. Ashby, D. Cebon, Materials selection in mechanical design, J. Phys. IV 3 (1993) 1–9.
[36] D.R. Lesuer, C.K. Syn, O.D. Sherby, J. Wadsworth, J.J. Lewandowski, W.H. Hunt, Mechanical behaviour of laminated metal composites, Int. Mater. Rev. 41 (1996) 169–197.